Tomographic Images of *P* Wave Velocity Variation at Parkfield, California

JONATHAN M. LEES[1] AND PETER E. MALIN[2]

Institute for Crustal Studies, University of California, Santa Barbara

Tomographic inversion is applied to delay times from local earthquakes to image three dimensional velocity variations near Parkfield, California. The 25 × 20 square km region is represented by nearly cubic blocks of 0.5 km per side. Arrival times of *P* waves from 551 local earthquakes, with depths of 0 to 15 km, were used as sources producing 3135 rays covering the target region. The data were recorded on low-noise downhole seismographs. A conjugate gradient method is used to invert the resulting sparse system of simultaneous equations. To diminish the effects of noisy data, the Laplacian of the model parameters is constrained to be small within horizontal layers, providing smoothing of the model. The resolution of the model is estimated by calculating point spread functions at blocks of interest. Estimates of standard errors of the model parameters are calculated by the jackknife statistical procedure. The results of the inversion show correlation with some of the local geological and geophysical features. Station corrections removed the long-wavelength anomaly associated with the contrast of the Salinian block southwest of the San Andreas fault versus the Franciscan to the northeast. A velocity low located a few kilometers northwest of Parkfield (depth 2.5-3.5 km), appears to lie along the gradient of the large Bouguer gravity anomaly associated with the Parkfield syncline. The south-southeastward extension of the low velocities may relate to reflections observed on the Parkfield, Consortium for Continental Reflection Profiling (COCORP) lines. We speculate on the geological meaning of these features and interpret them either as part of the local strike slip tectonics or a shallow crustal detachment. The correlation of higher-velocity features and seismic activity may indicate that earthquakes are occurring in more competent zones while aseismic slip takes place in zones of lower-velocity, less competent rocks.

INTRODUCTION

We have determined a three dimensional velocity model near Parkfield, California, using tomographic techniques applied to *P* wave data from an eight station downhole seismic network (Figure 1; *Malin et al.* [1989]). The tomographic inversion is based on methods of *Lees and Crosson* [1989], where linear inversion of *P* wave travel times is used to calculate the first order, three-dimensional slowness perturbations from the initial, one-dimensional reference model. The resulting images agree with previous velocity variation studies [*Eaton et al.*, 1970; *Michelini et al.*, 1989] and, further, have features that appear to relate to the local geology.

The geology of the Parkfield area is dominated by the San Andreas fault system [*Sims*, 1990; *Sims and Hamilton*, 1990]. The Salinian block on the southwest side of the San Andreas fault consists of Gabilan plutonic and metamorphic basement rocks covered by a maximum of 2 km of Tertiary and Quaternary marine and nonmarine sediments and volcanics. These deposits generally dip westward away from the Cholame Hills high, a basement uplift that lies several kilometers southwest and parallel to the San Andreas fault

system (Figure 1). Northeast of the San Andreas fault, the basement is widely exposed and consists of Franciscan melange, locally including mafic, ultramafic, and serpentinized rocks. Overlying this basement are several kilometers of Cretaceous and younger sediments of the Great Valley sequence. In the study area the latter rocks are contained in the broadly folded Parkfield Syncline, over which the basement has been thrust from the northeast by the Table Mountain fault.

Three other faults play varying roles in the local geology (Figure 1). The Gold Hill fault immediately northeast of the San Andreas fault is mapped as a southwest dipping thrust [*Sims*, 1990; *Sims and Hamilton*, 1990]. The Southwest Fracture Zone immediately southwest of the San Andreas fault exhibited moderate right-lateral surface displacement in the 1966 Parkfield earthquake [*Brown et al.*, 1967]. Several kilometers further to the south, the Parkfield segment of the San Andreas fault may have a buried, older branch related to the mapped White Canyon fault in the Cholame Valley, which lies outside our target area [*Sims and Hamilton*, 1990].

Both the Parkfield Syncline and the broad Cholame Hills high can be observed as local gravity anomalies (Figure 2; *Hanna et al.* [1972]). The gravity low east of station MM reflects the northwestward plunge of low-density sediments of the Parkfield Syncline. The gravity high associated with the Cholame Hills high uplift of Salinian basement turns from a southeast trend toward the southwest near seismic station Vineyard Canyon (VC). From the latter point the basement slopes down to the west and northwest with commensurate thickening of the sedimentary cover.

Previous earthquake studies of the Parkfield region have produced one-, two-, and three-dimensional velocity models. The U.S. Geological Survey (USGS) routinely locates local earthquakes using the California Network (CALNET) array

[1]Now at Department of Geology and Geophysics, Yale University, New Haven, Connecticut.

[2]Now at Department of Geology, Duke University, Durham, North Carolina.
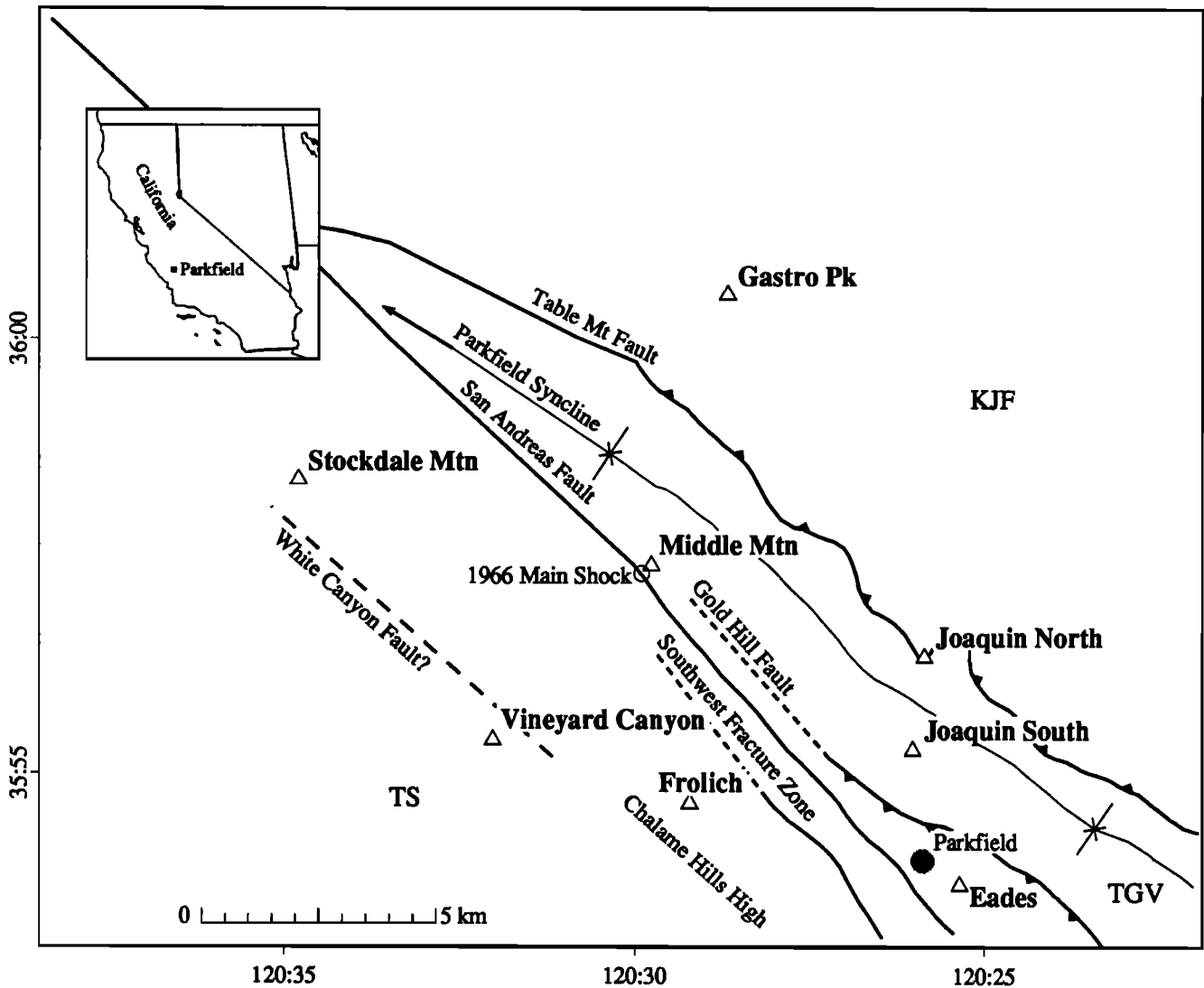
Fig. 1. Map of target area and station distribution of the Parkfield downhole seismic network. Triangles are station locations. The major geological features discussed in the text, such as the San Andreas fault, Gold Hill fault, Southwest Fracture Zone, White Canyon fault and Parkfield Syncline, are also indicated. Major geologic units include KJF, Franciscan basement; TGV, Tertiary Great Valley sediments; TS, Tertiary cover over Salinian basement. The small solid square indicated on the inset map is the area of the target region.

with the one-dimensional velocity model similar to that shown in Table 1 and Figure 3a [*Nowack et al.*, 1980; *Nishioka and Michael*, 1990]. Station corrections were determined by iterating between hypocenter locations and adjustment of an average station residual such that travel time residuals for each station became small. Using aftershocks of the 1966 earthquake, *Eaton et al.* [1970] determined two separate velocity structures for each side of the San Andreas fault between Parkfield and Cholame. To a depth of ~4 km the velocity on the southwest side was found to be lower at the surface, but more rapidly increasing, than on the northeast side. Below 4 km depth the velocities on both sides of the fault were the same. Using surface vibroseis and 75 events selected from the same data set discussed here, *Michelini et al.* [1989] found a three dimensional *P* and *S* wave velocity model along the San Andreas fault north of *Eaton et al.* [1970]. The three-dimensional model consists of

144 velocity nodes in a 20 km long, 10 km wide, and 15 km deep volume centered on the epicenter of the 1966 earthquake. Below ~1 km depth the southwest side of the fault was found to have significantly higher velocity to a depth of 15 km. *S* wave data indicated a low-velocity feature of 1 km width along the fault zone. *Michelini et al.* [1989] also observed a planar zone of several square kilometers surrounding the 1966 mainshock hypocenter which exhibited increased Poisson's ratio.

A Consortium for Continental Reflection Profiling (COCORP) seismic reflection profile has been recorded in the southeastern portion of the study region (Figure 2; *Long* [1981]; *McBride and Brown* [1986]). Standard processing and prestack migration CMP sections revealed reflections from the Parkfield Syncline and a 2-4 km deep zone between the Gold Hill fault and the Southwest Fracture Zone (Figure 4; *Louie et al.* [1988]). These data contain deeper reflections
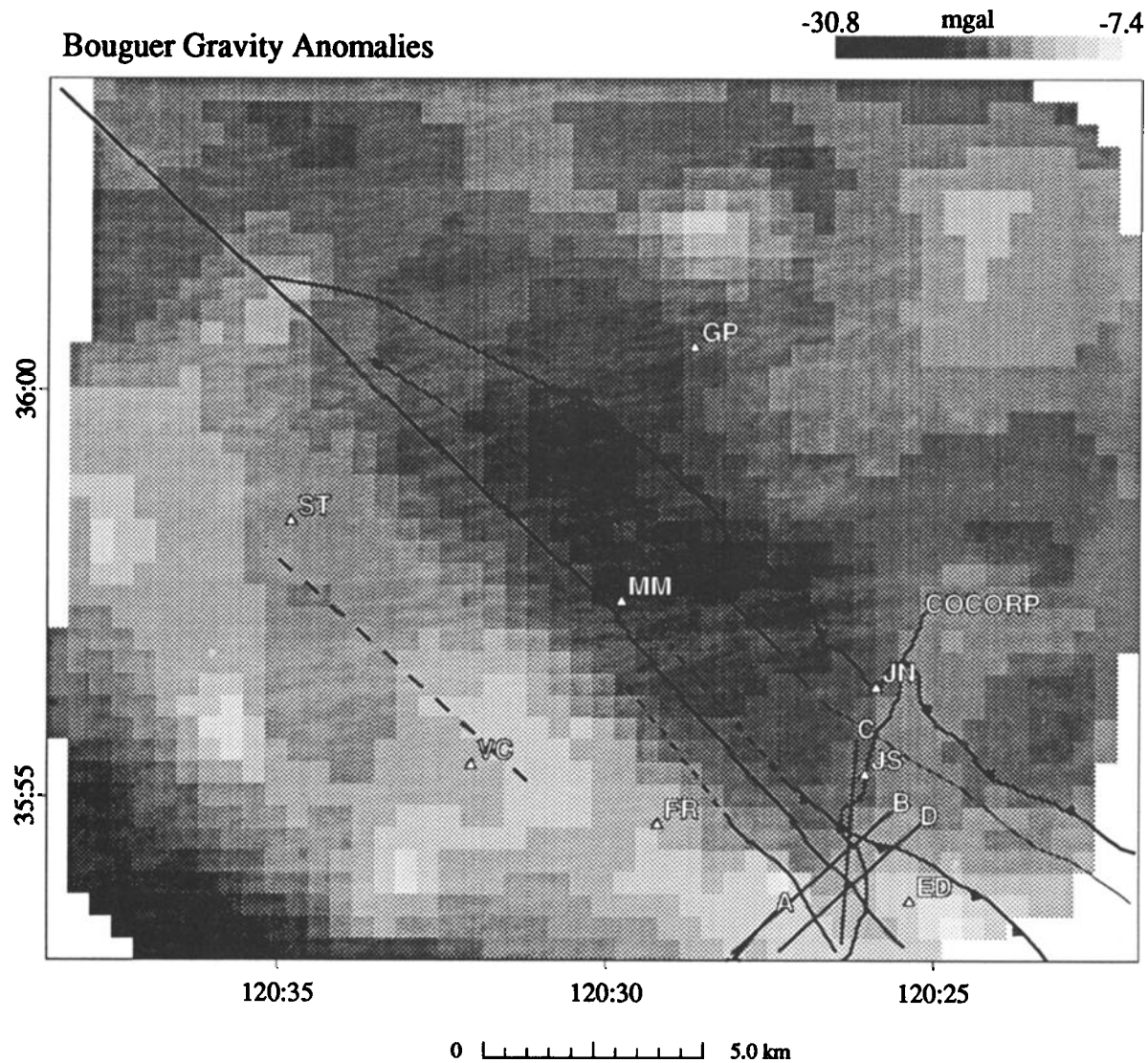
Bouguer Gravity Anomalies

Fig. 2. Bouguer gravity anomalies for the Parkfield region. Dark regions represent low-gravity perturbations, and lighter regions correspond to high gravity. The traces of four seismic common midpoint (CMP) sections, along the COCORP line, are plotted as A-D [from *Louie et al.*, 1988]. Station locations are ED, Eades; FR, Frolich; GP, Gastro Peak; JN, Joaquin North; JS, Joaquin South; MM, Middle Mountain; ST, Stockdale Mountain; and VC, Vineyard Canyon.

TABLE 1. Parkfield Velocity Model

Layer	Depth, km	Reference Velocity	USGS Model	Minimum %Slowness	Maximum %Slowness	Minimum Velocity	Maximum Velocity	-5% Velocity	+5% Velocity
1	0.00	1.42	1.42	-0.29	0.96	1.41	1.42	1.35	1.49
2	0.25	3.24	3.24	-2.87	6.51	3.04	3.34	3.09	3.41
3	1.50	4.82	4.82	-8.20	12.35	4.29	5.25	4.59	5.07
4	2.00	5.09		-7.54	8.48	4.69	5.51	4.85	5.36
5	2.50	5.36	5.36	-6.08	8.51	4.94	5.71	5.10	5.64
6	3.00	5.48		-8.69	12.75	4.86	6.00	5.22	5.77
7	3.50	5.60	5.60	-6.00	6.89	5.24	5.96	5.33	5.89
8	4.75	5.73		-5.35	4.32	5.49	6.05	5.46	6.03
9	6.00	5.87	5.87	-5.13	5.45	5.57	6.19	5.59	6.18
10	7.50	6.01		-4.94	5.77	5.68	6.32	5.72	6.33
11	9.00	6.15	6.15	-5.07	3.30	5.95	6.48	5.86	6.47
12	12.00	6.38		-1.68	1.23	6.30	6.49	6.08	6.72

Velocities are in kilometers per second. Columns 5 and 6 represent the maximum and minimum percent perturations for the given layers and columns 7 and 8 are the corresponding velocities for the respective extreme perturbations. Columns 9 and 10 are the velocities for ±5% perturbation anomalies as plotted in Figure 4.

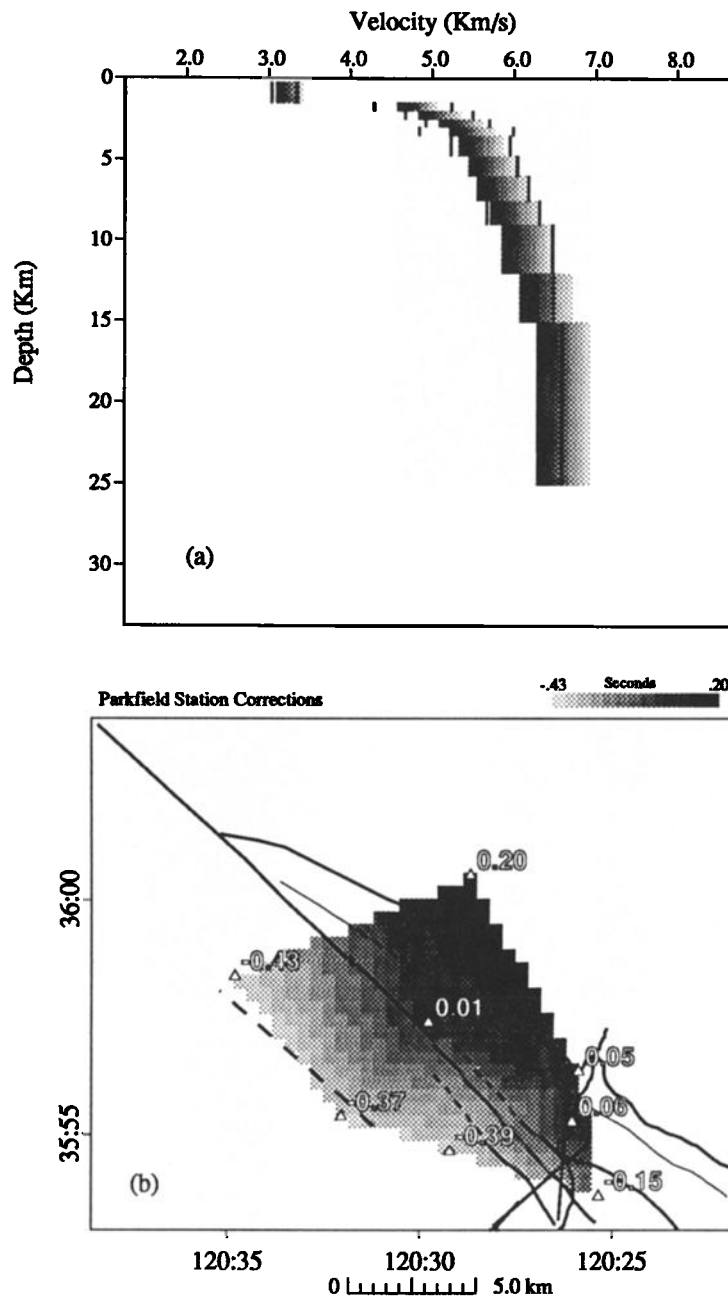Fig. 3. (*a*) Vertical profiles of the initial and final velocities of the tomographic inversion procedure. The grayshade bars represent the ±5% anomalies plotted in Figure 5. The initial velocity model used for the earthquake locations lies at the center of the grayshade bar. The actual maximum and minimum velocity variations found in the tomographic inversion are shown by vertical bars in each layer, with the largest variation lying in layer 5. (*b*) Interpolation of station corrections at the stations (open triangles) of the network. Notice trend of decreasing velocity towards the northeast across the San Andreas fault.

interpreted as the bases of the Salinian and Franciscan blocks at 10 and 15 km depth, respectively.

Drill hole data near the COCORP profile at the Gold Hill fault suggest the Parkfield Syncline is 2 km deep with a basement of Franciscan rocks (profile C, Figure 4; Malin et al. [1987]). Southwest of the Southwest Fracture Zone in the Salinian block, drill hole and reflection data indicates the top of the Salinian is at 2.5 km depth (profile A, Figure 4). Between the Gold Hill fault and the Southwest Fracture Zone,

where no drill hole data are available, reflections are observed at 3.5 km depth, appearing to pass under the surface exposure of the San Andreas fault (profile B, Figure 4).

DATA SET AND TOMOGRAPHIC INVERSION

The 3135 *P* wave travel times of the 551 microearthquakes used in our study were recorded from 1987 to 1989 with a digitization rate of 500 Hz. While the
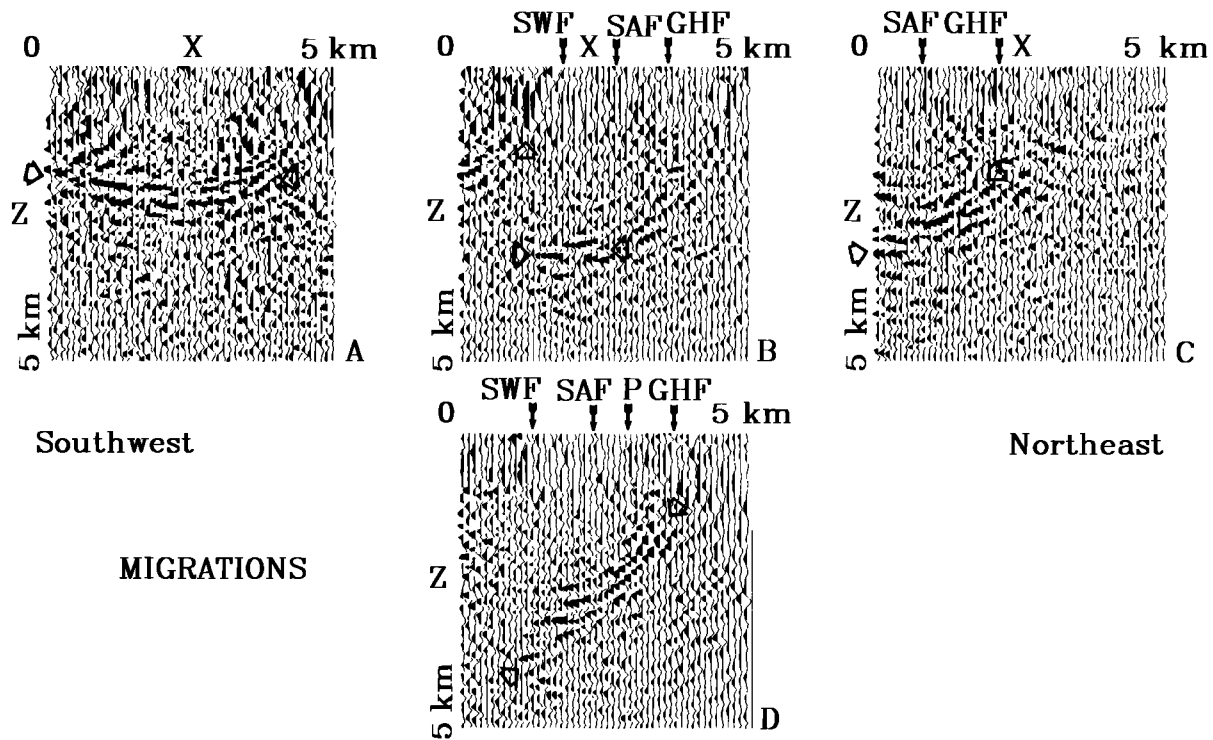
Fig. 4. Four prestack migration CMP sections along the profiles plotted in Figure 2 [Louie et al., 1988]. Note the horizon at 3 km depth in section B spans the fault.

relative magnitudes of these small events ranged from -0.5 < M_{local} < 1.5, the low noise downhole seismograms allowed first arrivals to be picked in most cases to ±0.005 s. Only data whose entire raypath remained in the target volume (Figure 1) were included in the inversion. The initial one-dimensional reference model and station corrections were provided by the USGS (A. J. Michael, USGS, Menlo Park, 1989, personal communication). Roughly one third of the hypocenters included in our study lie outside of the geometric limits bounded by the station network (Figure 5a) although we found that this did not affect the inversion results significantly.

Several layers of the initial USGS one-dimensional reference model were subdivided into two equal parts with equal steps in velocity to achieve finer parameterization with depth (Table 1 and Figure 3a). Station corrections were redetermined by iterative recalculation of hypocenters and station delays until nearly zero-mean, symmetric distributions of station residuals were achieved for each site [Lees and Crosson, 1989]. Effectively, this removed gross velocity differences across the two sides of the San Andreas fault (Figure 3b). The target volume was divided into 50 × 40, 0.5 square km blocks with 12 layers in depth following the one-dimensional reference velocity model, providing a maximum of 24,000 model parameters. Rays were traced through the one-dimensional model and first-order perturbations of slowness were calculated in each block such that the sum of the squared travel time residuals (observed minus predicted) is minimized in a single, first-order linear adjustment [Aki et al., 1977; Humphreys and Clayton, 1988]. The data were weighted according to estimates of picking error and, to some extent, according to their spatial

distribution such that clusters of rays were downweighted to achieve a more homogeneous ray distribution [Lees and Crosson, 1989]. We have reduced the effects of noisy data by constraining the Laplacian (second spatial derivative) of the slowness field to be small within horizontal layers, which effectively smooths the model laterally [Lees and Crosson, 1989]. This is controlled by a damping parameter, $\lambda = 600$, chosen by trial and error, such that a reasonable amount of misfit reduction and model smoothing was attained. While it is likely there remains residual structure in the data, which we have not explained with our three-dimensional model, we do not have a good estimate for the expected errors due to nonlinearities and parameterization. For this reason we have not reduced the misfit of the data to the relatively low level of estimated noise observed in the travel time picks. The resulting system of simultaneous equations was solved by a conjugate gradient technique (LSQR) developed by Paige and Saunders [1982]. After 30 steps in the search the sum of squared travel time residuals was reduced to nearly half (46%) its initial value.

Several experiments were performed to test for dependance of the images on the parameterization. We reduced the initial block size both horizontally and vertically and found the gross features of the model to be stable. Inversions were performed excluding data from the northwest portion of the target where seismicity is dispersed and locations are poorly constrained. We found no evidence that these poorly constrained events seriously effected anomalies located within the bounds of the network. To determine the influence of the variability of the data on the model, we performed a jackknife error analysis [Lees and Crosson, 1989; Tichelaar and Ruff, 1989]. The standard errors (1 σ)
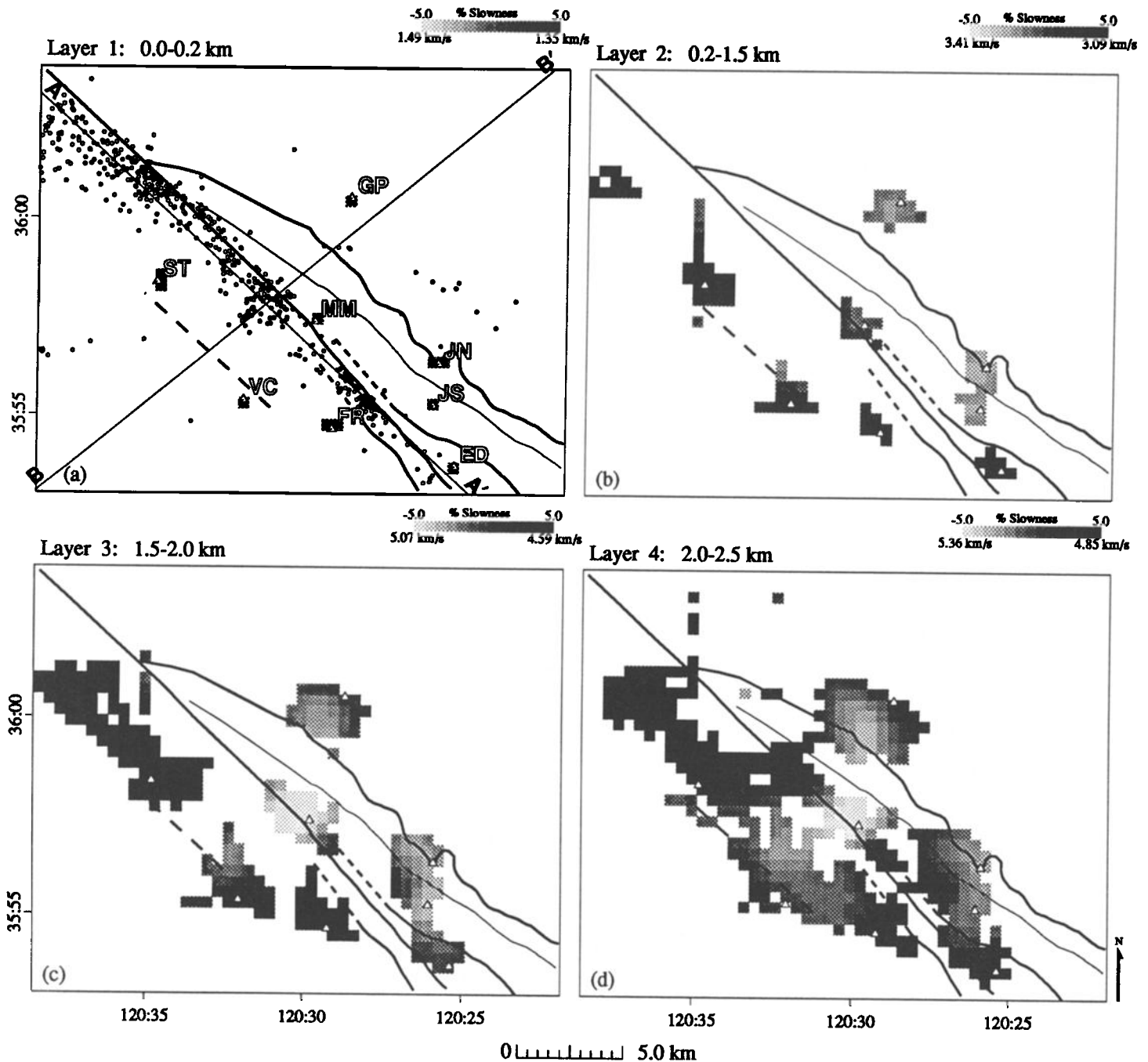
Fig. 5. (a-l)Tomographic inversion for Parkfield, California. The horizontal cross sections are partitioned according to the one-dimensional reference velocity model. Dark areas represent zones of low-velocity perturbations (high slowness) and light shades represent high-velocity anomalies (low slowness). Figure 5a includes a plot of the epicenters (open circles) used as sources for the inversion. The map view of the cross sections of Figure 6 is also included in Figure 5a. Station abbreviations in Figure 5a are the same as in Figure 2. Open triangles are station locations.

calculated in this manner were found to be typically 1% or less (slowness perturbation) over most of the model, suggesting slowness variations greater than a couple of percent are significant. The resolution for one block can be calculated by placing a unit spike in the block (i.e., slowness perturbation = 1 in one block), computing the forward travel times through the spike model and inverting

the output. The result is the impulse response (point spread function) of the system (data + inversion + smoothing) for that block. Impulse responses for different parts of the model were calculated to determine the overall resolution. Near the center of the model, where the ray coverage is most dense, the lateral resolution length was found to be slightly better than 2 km (3-4 blocks). The resolution kernels, however, are
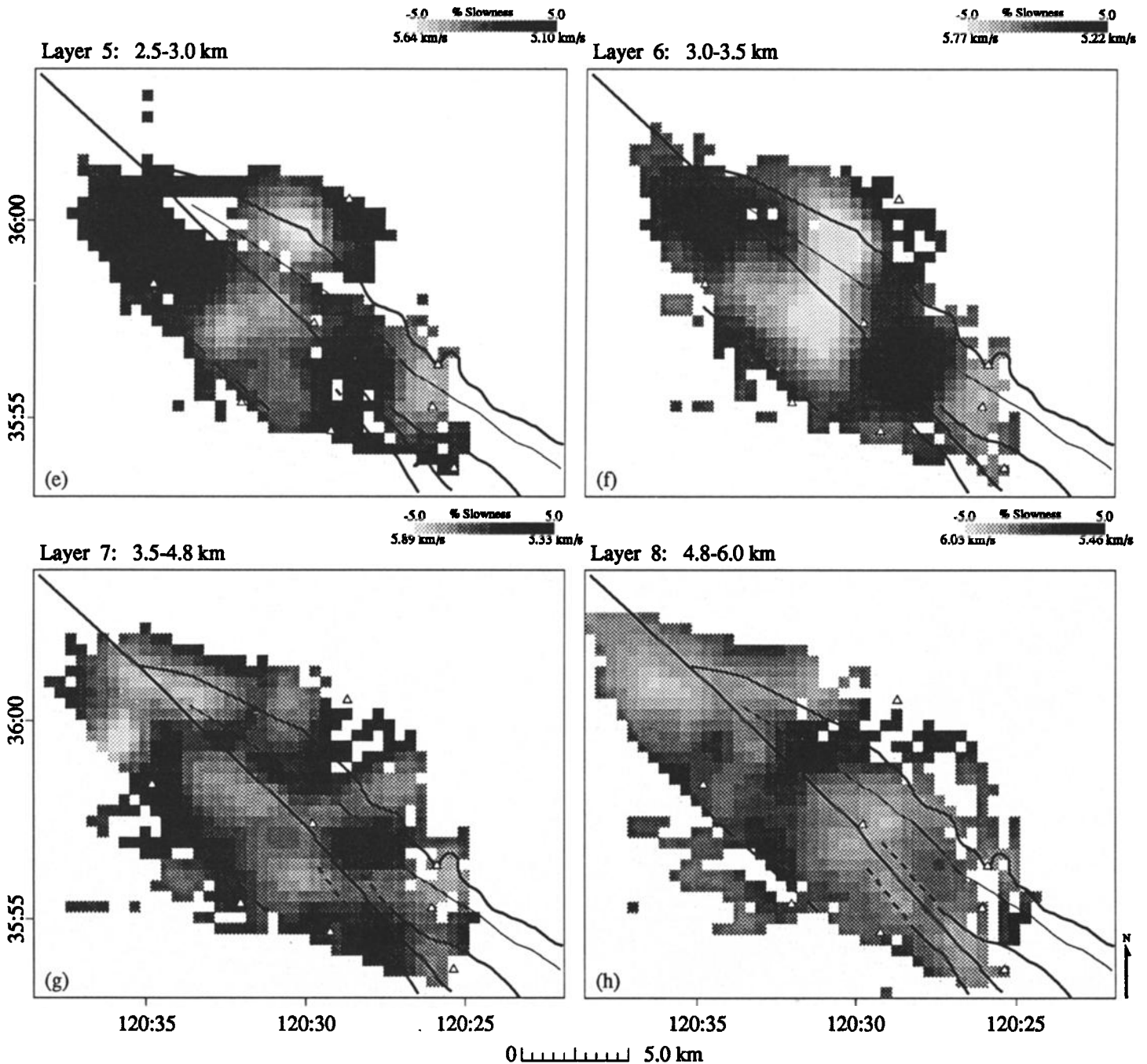
Fig. 5. (continued)

typically not symmetric, due to heterogeneity of ray coverage. Because the seismicity is generally aligned in a NW-SE direction, there is smearing of less constrained anomalies in this direction.

To display results of the inversion, grayshade plots were created for each layer (Figures 5a-5l) and for two cross sections (Figures 6a-6d). Since we have derived a three-dimensional perturbation model, we prefer to display the results as perturbations from the background reference velocity, as opposed to absolute velocity values. In this way the average one dimensional model, which would otherwise dominate the image, is removed. (For the two cross sections

we have provided contour plots of the absolute velocities in Figures 6c and 6d) The perturbations have been plotted with a common, fixed grayscale ranging from -5% to 5% slowness. The true limits of the grayscale, however, vary from layer to layer. The extreme perturbation values and their respective absolute velocities for each layer are shown in Figure 3a. The dark shades represent blocks whose slowness is anomalously high (low velocity), and lighter shades correspond to anomalously lower slowness (high velocity). To indicate where raypaths did not constrain the inversion, blocks that were not penetrated by any rays appear as white space on the plots.
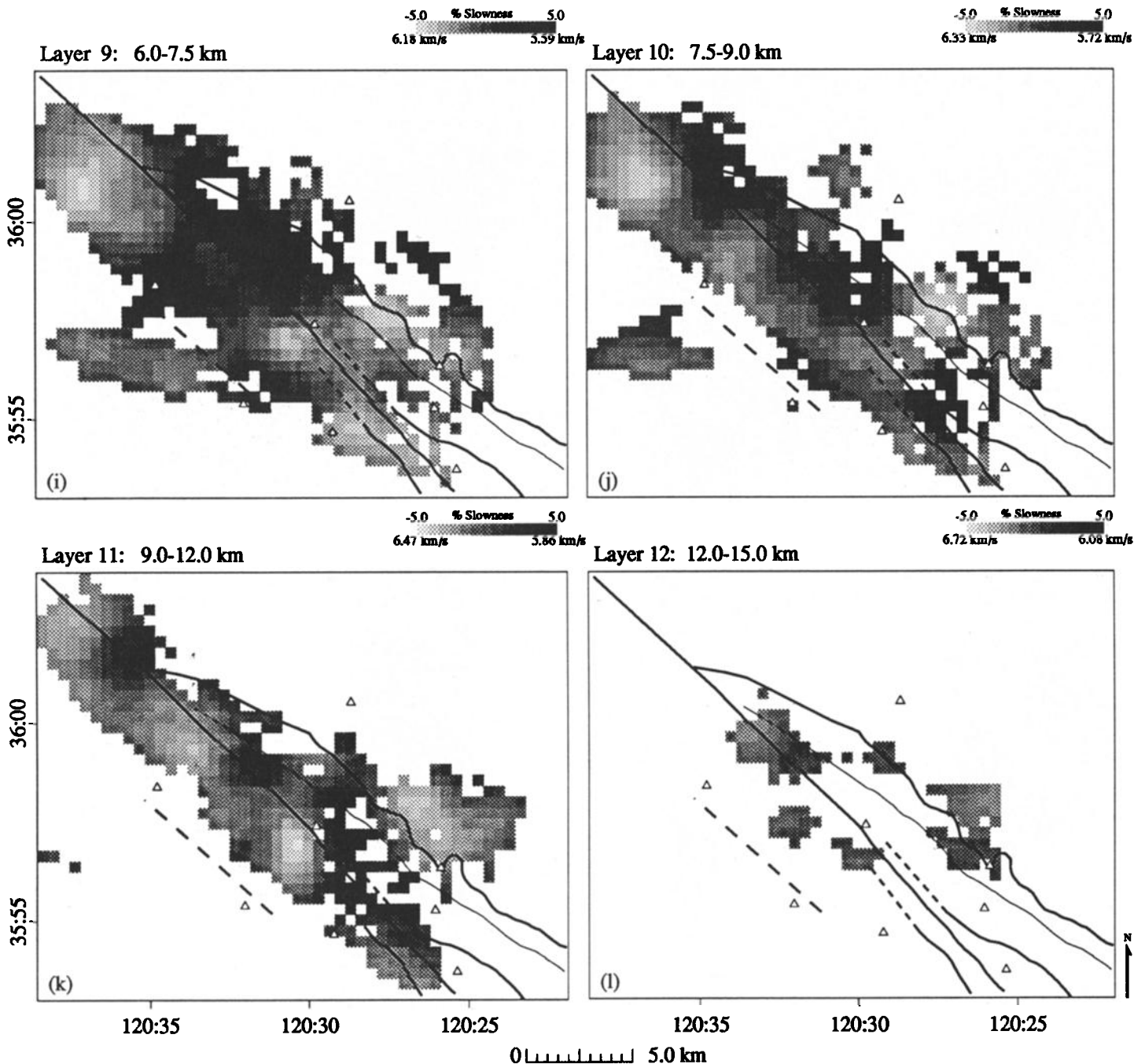
Fig. 5. (continued)

RESULTS

The three shallowest layers of the model (<2.0 km) have poor lateral resolution because emerging rays tend to cluster near observation points. In these layers an apparent trend of lower velocities exists southwest of the San Andreas fault. There are corresponding higher velocities beneath stations to the northeast. These trends are small compared to the station corrections (equivalent to 5% versus 50-100% perturbation in layer 1 slowness) and may be considered residual site effects not accounted for by the station corrections.

Below 2.0 km the spatial resolution of the image is higher. In the northwest by station ST, a broad low-velocity (5.0 %) anomaly is apparent from 2.0 to 3.5 km depth. This anomaly reverses itself below 3.5 km depth and remains an apparently northwest dipping high velocity perturbation to a depth of 12.0 km (see cross section AA' in Figure 6a). At 2.5-3.5 km depth (layers 5 and 6), high-velocity anomalies appear on both sides of the San Andreas fault northwest of station MM. These features either terminate at 3.5-4.8 km depth or they represent the shallow extension of the deeper northwest high-velocity anomaly just mentioned. Southeast of MM, between 2.0-3.5 km depth, a low-velocity feature
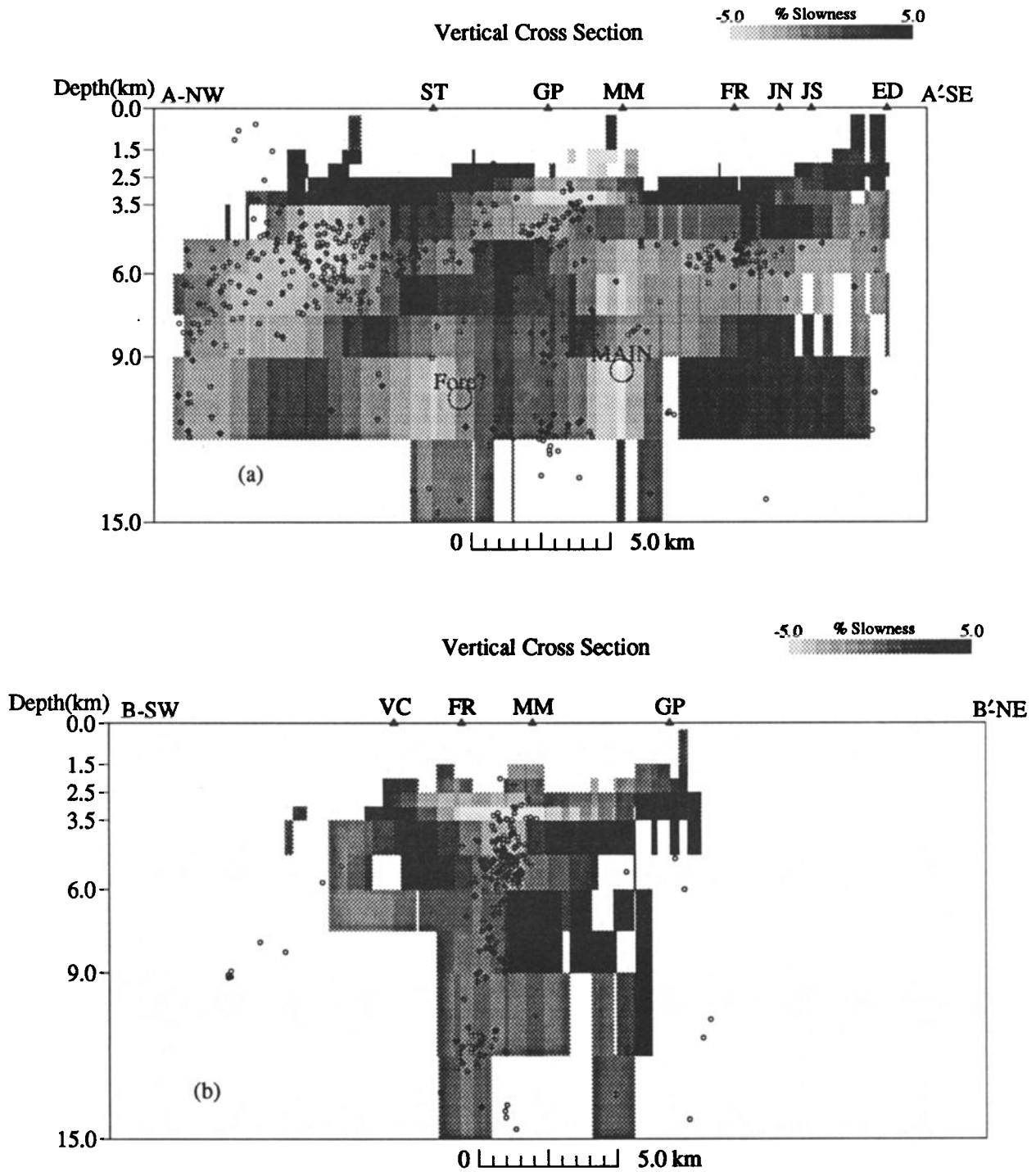
Fig. 6. Cross sections through the three-dimensional model. Map view of cross sections is displayed in Figure 5a. Station abbreviations are the same as in Figure 2. (a) Cross section AA' runs parallel to the San Andreas fault along the zone of highest seismicity. Hypocenters are projected on the vertical section along with the stations at the surface for reference. (b) Section BB' is perpendicular to the San Andreas fault, bisecting it near station MM. Notice the correlation of the seismicity to the higher-velocity regions and the fast, but currently quiet, fault patches near the 1966 main shock and foreshocks. (c) Contour plot of actual velocities corresponding to cross section AA'. (d) Contour plot of actual velocities corresponding to cross section BB'.
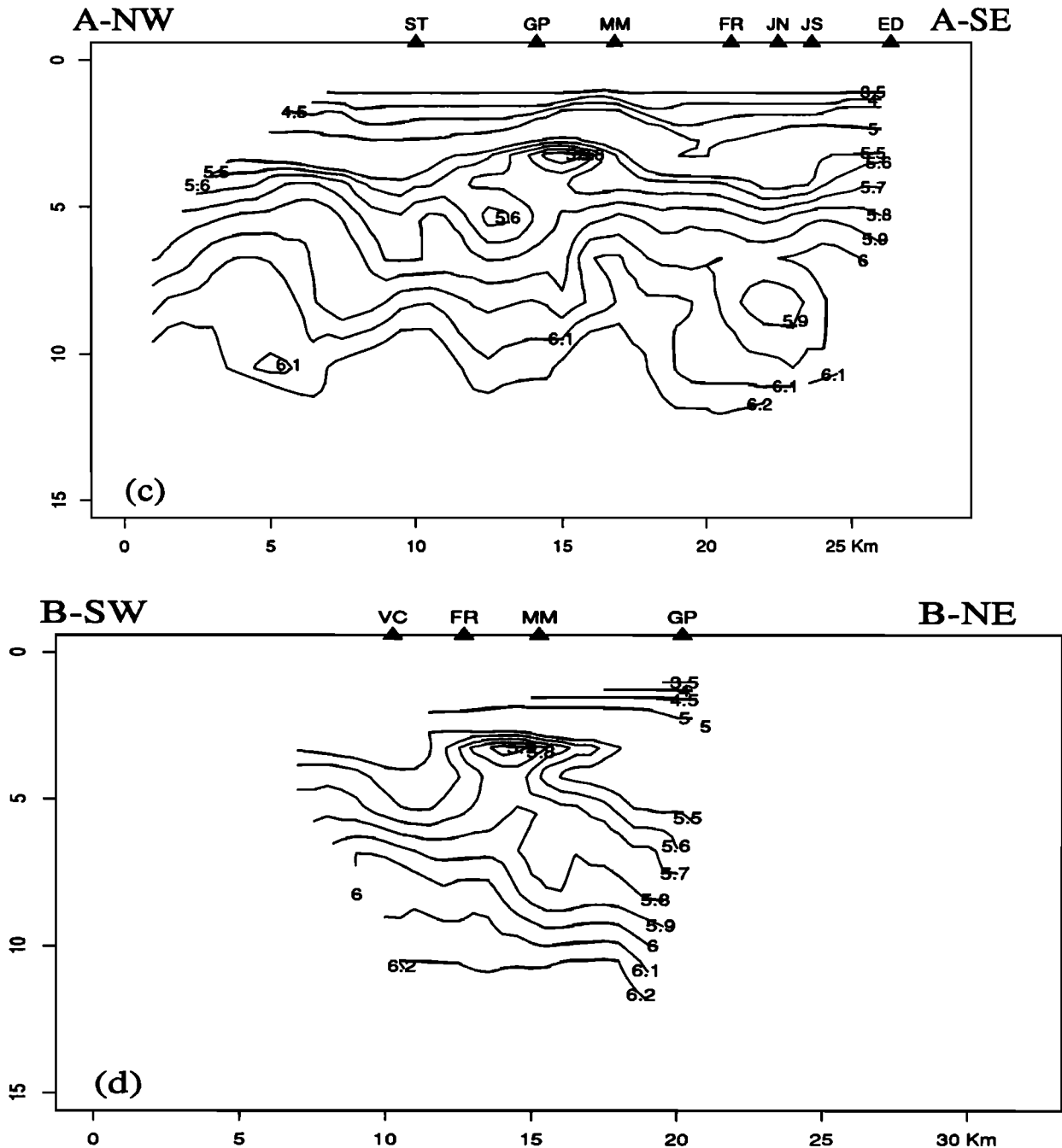
Fig. 6. (continued)

(cut off at 5% in Figure 5e, but with an actual maximum of 12.75%) appears to span the San Andreas fault zone. There is little evidence that this feature continues below 4.8 km depth.

An apparent transition zone is observed between layer 7 (3.5-4.8 km depth) and layer 8 (4.8-6.0 km depth). Velocity anomalies in layer 7 exhibit a demarcation between high and low velocities which trends subparallel to the San Andreas fault. On the northeast, two low-velocity anomalies are observed between the Table Mountain and the San Andreas faults. A higher-velocity feature is observed at the junction of these two faults. Southwest of the San Andreas fault, we observe a ridge of higher velocity adjacent to the fault and lower velocities near the edge of the model further to the southwest, between stations Vineyard Canyon (VC) and Stockdale Mountain (ST). In cross section these variations define a northeast dipping trend down to 6 km depth (see also the southwest end of cross section BB' in Figure 6b). In the 4.8-7.5 km depth range (layers 8 and 9) the velocity variations appear to broaden laterally, with higher values to the southeast and northwest separated by a low values between stations ST and Gastro Peak (GP). Below 7.5 km

depth we observe a general trend of higher velocity anomalies southwest of the San Andreas and lower velocities to the northeast, although ray coverage generally degrades at depth.

The spatial relation of the velocity variations and earthquake seismicity is shown on profiles AA' and BB' in Figures 6a and 6b. Cross section AA', taken parallel to the San Andreas along the line of densest seismicity, exhibits a correlation of low-velocity anomalies to low seismicity. Seismicity is apparently restricted to regions of higher velocity, although not all zones of high velocity have associated high seismicity. In cross section BB', normal to the San Andreas fault near Middle Mountain (MM), the seismically active zone apparently dips to the southwest in agreement with previous studies by Eaton et al. [1970], Lindh and Boore [1981], Nishioka and Michael [1990], and Michelini et al. [1989]. Cross section BB' also indicates that regions of high seismicity correlate with higher velocity anomalies.

DISCUSSION

The sparsely sampled top kilometers of the three-dimensional velocity model display a trend of lower velocity to the southwest and higher velocity to the northeast. We interpret these perturbations as residual adjustments to the station corrections which were applied to the total travel times prior to inversion. The trend of the station corrections indicates lower velocity on the southwestern Salinian block in contrast to the higher velocity Franciscan rocks to the northeast. While we cannot say specifically what the source of the station correction is, the fact that the signal in the station corrections is considerably longer wavelength than the observed signal in the inversion indicates that this trend is most likely due to the long wavelength structure pertaining to the regional difference between the Franciscan and Salinian blocks. (Corrections due to elevation variations are considerably smaller than the station corrections we have used.) We suspect the corrections relate primarily to structure above 2-3 km depth since the shallow structure of our model has an apparent cross fault, long wavelength, regional correction to these terms. Considering that the top of the Salinian block is composed of undeformed shallow marine and valley fill deposits in contrast to metamorphosed basement exposures in the northeast Franciscan block, we surmise that the trends observed in our results are reasonable.

On the basis of surface geology and drill hole data the Parkfield Syncline is a tightly folded structure that plunges to the northwest between the Gold Hill and Table Mountain thrust faults. While the subsurface configuration of the syncline is not known, the gravity data suggests its deepest part lies to the north of MM (Figure 2). The "half width" of the gravity anomaly indicates its source extends no deeper than 4 to 6 km or so [Dobrin, 1960], correlating possibly with the lower velocities seen in the same position in layers 7, 8, and 9 (3.5 to 7.5 km deep; see also cross sections AA' and BB'). The shallow low-velocity anomaly found in layers 5 and 6 (2.5 to 3.5 km), southeast of MM, does not appear to correlate with the gravity anomaly as we might have expected. In this zone there appears to be a high-velocity anomaly where the gravity is lowest and the low-velocity anomaly is situated along the gravity gradient. The

COCORP line on the southeastern edge of our target area suggests that a horizontal velocity contrast at 3.5 km depth underlies the surface trace of the San Andreas fault (profile B, Figure 4; Louie et al. [1988]). The character of the reflections from this horizon appear similar to those from the known basement-sediment contacts on either side (profiles A and C, Figure 4). The velocity low in layers 5 and 6 southeast of MM also spans the San Andreas fault. If the gravity and velocity lows were directly correlated and extended southeastward toward the COCORP line, then it would be possible to speculate that these features were produced by local transtensional downdropping of the Salinian and Franciscan basements, with a corresponding thickening of the overlying, lower-density sediments. This evidentially not being the case, the low velocities in layers 5 and 6, and by inference the COCORP reflector, may relate to the interaction of the Southwest Fracture Zone and Gold Hill fault with the San Andreas, possibly in the from of a shallow crustal detachment (see also McBride and Brown, 1986]. This low-velocity feature is similar to a low-velocity anomaly, observed southeast of the 1989 Loma Prieta earthquake [Lees, 1990a; Lees, 1990b], which also appears to span the surface trace of the San Andreas fault.

Along the San Andreas fault itself, one might expect a low velocity lineation to be associated with its zone of fault gouge and crushed rocks [Michelini et al., 1989]. We have not observed this phenomenon, although we do observe a demarcation along the fault separating the Salinian and Franciscan blocks, particularly in the deeper layers (3.5-12 km depths). The lack of a definitive, laterally continuous fault zone may be due to both the resolution of our method and heterogeneous structure. Since the resolution of our inversion is approximately 2 km in the center of the model, a fault gouge at least this thick would be required to be observable with any degree of confidence.

The only particularly linear feature in the tomographic images is the east dipping low-velocity band we noted on its southwestern edge (best seen in cross section BB', Figure 6b). While this is near the edge of our model, where the resolution is degraded, we suspect this feature is real and note that the northward extension of the White Canyon fault, which may have been a previous main break of the San Andreas, has been suggested to lie in this area [Sims, 1990; Sims and Hamilton, 1990].

We note that low- and high-velocity variations image seismic and aseismic zones along the San Andreas fault zone (cross section AA', Figure 6). Since nearly all the seismicity is associated with higher-velocity anomalies, we propose that higher-velocity features represent brittle, and thus seismogenic, structures, in contrast to the more ductile, aseismic, structures of lower velocity. This trend contrasts that observed near Mount St. Helens [Lees and Crosson, 1989], where seismicity is associated with lower-velocity regions, suggesting that the correlation of seismicity with velocity structure is not an artifact of the technique but an indicator of tectonic style. Two deep (9-12 km depth), high-velocity regions that do not contain numerous small earthquakes correlate with the main shock and possible foreshock patches of the 1966 earthquake sequence (see also Michelini et al. [1989], Malin et al. [1989], and Bakun and McEvilly [1984]). The greater shear strength observed by Michelini et al. [1989] supports our interpretation that the volume surrounding the 1966 main shock is comprised of

competent material. We anticipate that these represent locked zones where future seismicity is likely to occur.

CONCLUSIONS

We have used tomographic inversion methods to calculate a three-dimensional velocity variation model for Parkfield, California. Impulse response tests and different parameterizations of the velocity structure indicate the lateral resolution is ~2 km near the center of the model. Jackknife estimates of the model parameter errors indicate that velocity variations larger than 2% are statistically significant.

We have observed northwest dipping low- and high-velocity variations northwest of Middle Mountain. An apparent transition zone exists at 4.8 km depth, below which the variations become laterally broader. The plunge of the Parkfield Syncline seems to have a dramatic affect on the gravity along it, producing an anomalous low between the Table Mountain and San Andreas faults. This anomaly may correlate with low-velocities at a depth of roughly 5 km. However, the relation of low density and low velocity does not appear to hold for the largest low-velocity perturbation southeast of Middle Mountain, where the low velocities lie a a gravity gradient. We have discussed the possibility that this transition zone may correlate with strong, slightly shallower reflections observed on COCORP seismic profiles on the southern edge of our model. We also discussed the possible origin of these features either as a down drop in the local basement rocks due to strike slip tectonics or, more likely, a shallow detachment.

High seismicity is dominantly located in higher-velocity regions, suggesting a correlation of microearthquakes with seismically competent, presumably more brittle materials. In contrast, few earthquakes used in our study are associated with low-velocity anomalies, suggesting a correlation with seismically incompetent material. In this interpretation, the high-velocity, currently inactive, fault patches near the hypocenters of the foreshocks and main shocks of the 1966 Parkfield earthquakes may become centers of future earthquake activity.

REFERENCES

Aki, K., A. Christoffersson, and E. S. Husebye, Determination of the three-dimensional seismic structure of the lithosphere, *J. Geophys. Res., 82*, 277-296, 1977.

Bakun, W. H., and T.V. McEvilly, Recurrence models and Parkfield, California, earthquakes, *J. Geophys. Res., 89*, 3051-3058, 1984.

Brown, R., Jr., J. G. Vedder, R. E. Wallace, E. F. Roth, R. F. Yerkes, R. O. Castle, A. O. Waananen, R. W. Page, and J. P. Eaton, The Parkfield-Cholame California, earthquakes of June-August 1966 - surface geologic effects water-resources aspects and preliminary seismic data, *U.S. Geol. Surv. Prof. Pap. 579,* 66 pp 1967.

Dobrin, M. B., *Introduction to Geophysical Prospecting,* 446 pp, McGraw-Hill, New York, 1960.

Eaton, J. P., M. E. O'Neill, and J. N. Murdock, Aftershocks of the 1966 Parkfield-Cholame, California, earthquake: A detailed study, *Bull. Seismol. Soc. Am., 60*(4), 1151-1197, 1970.

Hanna, W. F., S. H. Burch, and T. W. Dibblee, Gravity, magnetics, and geology of the San Andreas Fault area near Cholame, California, Geophysical Field Investigations, *Geol. Surv. Prof. Pap. 646-C,* 1972.

Humphreys, E., and R. W. Clayton, Adaptation of back projection tomography to seismic travel time problems, *J. Geophys. Res., 93,* 1073-1085, 1988.

Lees, J. M., Comparison of high resolution tomographic P-wave inversions at Parkfield and Loma Prieta, California, *Seismol. Res. Lett., 61,* 49, 1990a.

Lees, J. M., Tomographic P-wave velocity images of the Loma Prieta earthquake asperity, *Geophys. Res. Lett.,* 17, 1433-1436, 1990b.

Lees, J. M., and R. S. Crosson, Tomographic inversion for 3-D velocity structure at Mount St. Helens using earthquake data, *J. Geophys. Res., 94,* 5716-5728, 1989.

Lindh, A. G., and D. M. Boore, Control of rupture by fault geometry during the 1966 Parkfield earthquake, *Bull. Seismol. Soc. Am., 71,* 95-116, 1981.

Long, G. H., A COCORP deep seismic reflection profile across the San Andreas fault, Parkfield, California, M.Sc. thesis, Cornell Univ., Ithaca, N.Y., 1981.

Louie, J. N., R. W. Clayton, and R. J. LeBras, Three dimensional imaging of steeply dipping structure near the San Andreas fault, Parkfield, California, *Geophysics, 53,* 176-185, 1988.

Malin, P. E., T. V. McEvilly, and T. Moses, Cooperative UCSB-UCB-USGS recovery and instrumentation of the 5150ft Varian A-1 well as a geophysical observatory. *EOS Trans. AGU, 68*(44), 1357, 1987.

Malin, P. E., S. N. Blakeslee, M. G. Alvarez, and A. J. Martin, Microearthquake imaging of the Parkfield asperity, *Science, 244,* 557-559, 1989.

McBride, J.H., and L.D. Brown, Reanalysis of the COCORP deep seismic reflection profile across the San Andreas Fault, Parkfield, CA., *Bull. Seismol. Soc. Am., 76,* 1668-1686, 1986.

Michelini, A., W. Foxall, and T. V. McEvilly, The Parkfield monitoring program: Joint hypocentral and velocity inversion for three-dimensional structure, *Seismol. Res. Lett., 60,* 31, 1989.

Nishioka, G. K., and A. J. Michael, A detailed seismicity of the Middle Mountain zone at Parkfield, California, *Bull. Seismol. Soc. Am., 80,* 577-588, 1990.

Nowack, R., W. Ellsworth, and A. Lindh, Estimation of velocity structure in the vicinity of Parkfield, CA, *U. S. Geol. Surv., Open File Rep. 80-xx,* 77 pp, 1980.

Paige, C. C., and M. A. Saunders, LSQR: An algorithm for sparse linear equations and sparse least squares, *Trans. Math. Software, 8,* 43-71, 1982.

Sims, J. D., Geologic map of the San Andreas fault zone in the Parkfield 7.5 minute quadrangle, Monterey and Fresno Counties, California, *U.S. Geol. Surv. Misc. Field Stud. Map, MF-2015,* 1990.

Sims, J. D., and J. C. Hamilton, Geologic Map of the San Andreas fault in the Cholame Quadrangle, San Luis Obispo County, California, *U.S. Geol. Surv. Misc. Field Stud. Map, MF-XXXX,* in press, 1990.

Tichelaar, B. W., and L. J. Ruff, How good are our best models: Jackknifing, bootstrapping and earthquake depth, *EOS Trans. AGU, 70*(20), 593, 1989.

J. M. Lees, Department of Geology and Geophysics, Yale University, P.O. Box 6666, New Haven, CT 06511-8130.

P. E. Malin, Department of Geology, Duke University, Durham, NC 27706.